

## Radiation dominated implosion with nano-plasmonics

L.P. Csernai<sup>1</sup>, N. Kroo<sup>2,3</sup> and I. Papp<sup>4</sup><sup>1</sup>Department of Physics and Technology, University of Bergen, Bergen, Norway; <sup>2</sup>Hungarian Academy of Sciences, Budapest, Hungary; <sup>3</sup>Wigner Research Centre for Physics, Budapest, Hungary and <sup>4</sup>Department of Physics, Babes-Bolyai University, Cluj, Romania

## Research Article

**Cite this article:** Csernai LP, Kroo N, Papp I (2018). Radiation dominated implosion with nano-plasmonics. *Laser and Particle Beams* **36**, 171–178. <https://doi.org/10.1017/S0263034618000149>

Received: 28 November 2017

Revised: 14 March 2018

Accepted: 3 April 2018

**Key words:**

Inertial confinement fusion; nano-shells; relativistic fluid dynamics; time-like detonation

**Author for correspondence:**L.P. Csernai, Department of Physics and Technology, University of Bergen, Bergen, Norway. E-mail: [Laszlo.Csernai@uib.no](mailto:Laszlo.Csernai@uib.no)**Abstract**

Inertial Confinement Fusion is a promising option to provide massive, clean, and affordable energy for mankind in the future. The present status of research and development is hindered by hydrodynamical instabilities occurring at the intense compression of the target fuel by energetic laser beams. A recent patent combines advances in two fields: Detonations in relativistic fluid dynamics (RFD) and radiative energy deposition by plasmonic nano-shells. The initial compression of the target pellet can be decreased, not to reach the Rayleigh–Taylor or other instabilities, and rapid volume ignition can be achieved by a final and more energetic laser pulse, which can be as short as the penetration time of the light across the pellet. The reflectivity of the target can be made negligible as in the present direct drive and indirect drive experiments, and the absorptivity can be increased by one or two orders of magnitude by plasmonic nano-shells embedded in the target fuel. Thus, higher ignition temperature and radiation dominated dynamics can be achieved with the limited initial compression. Here, we propose that a short final light pulse can heat the target so that most of the interior will reach the ignition temperature simultaneously based on the results of RFD. This makes the development of any kind of instability impossible, which would prevent complete ignition of the target.

**Introduction**

Inertial confinement fusion (ICF) is an ongoing activity aiming for ignition of small pellets of thermonuclear, deuterium–tritium (DT) fuel by high-power lasers. The main direction of activity aims for strong compression of the fuel, where the resulting adiabatic heating would ignite the fuel. The pulse and the compression should be large and strong enough to keep the compressed fuel together for sufficient time for ignition, due to the inertia of the compressed pellet. This is the aim of both the direct drive (Nora *et al.*, 2015) and indirect drive experiments (Betti and Hurricane, 2016). In the present work, we present a patented idea on how to achieve final simultaneous volume ignition in the majority of the target based on recent theoretical and experimental achievements in relativistic fluid dynamics (RFD). (Csernai *et al.*, 2017).

In the pellet, the fusion reaction,  $D + T \rightarrow n(14.1 \text{ MeV}) + {}^4\text{He}(3.5 \text{ MeV})$ , takes place at a temperature of  $kT \approx 10 \text{ keV}$ . The produced  ${}^4\text{He}$  (or  $\alpha$ ) particles are then deposited in the hot DT plasma and heat it further. This is the plasma self-heating (or  $\alpha$ -heating). The compression wave penetrates into the plasma with the speed of sound or with the speed of a compression shock. There are several facilities with different configurations attempting to achieve nuclear fusion this way. A comprehensive summary of these is presented in Betti and Hurricane (2016). The goal of these experiments is to generate and sustain a self-propagating burn wave, which reaches the whole interior of the pellet.

The up to now most successful indirect drive configuration at the National Ignition Facility (NIF) the target capsule is indirectly ignited by the thermal radiation coming from the gold hohlraum. The hohlraum is heated by the radiation of 192 laser beams (Betti and Hurricane, 2016). In the middle of the hohlraum, a spherical pellet of DT fuel of initial outer radius of  $1143 \mu\text{m}$  is compressed and heated by the radiation. The pellet has a hole in the middle and a thin “ablator” layer, to reach better compression (Lindl, 1998; Lindl *et al.*, 2004; Haan *et al.*, 2011; Robey *et al.*, 2012). The incoming and reflected light exercised a pressure and compressed the pellet at NIF, to about  $R = 50 - 80 \mu\text{m}$  just before ignition. At this moment the hole in the capsule is already filled in, and the target density was compressed to about  $300 - 700 \text{ g/cm}^3$ , (Clark *et al.*, 2015; Reis *et al.*, 2016). In some cases, especially at the earlier “low foot” initial irradiation, this target showed the development of Rayleigh–Taylor (RT) instabilities, which reduced the efficiency of ignition. Recent simulations suggest that low foot performance was dominated by ablation front instability growth, high foot implosions appear to be dominated by hohlraum flux asymmetries (Clark *et al.*, 2016).

At NIF the initial compression pulse, the “foot” had a lower frequency or longer wavelength of 100–350 nm, and led to lower temperature irradiation in the hohlraum of  $T_{\text{RAD}} = 270 - 300$  eV (Glenzer *et al.*, 2011). This had a higher reflectivity on the target, and led to compression. The reflectivity of light is high ( $>0.6$ ) for lower energy irradiation and decreasing with increasing energies. It becomes negligible at  $\hbar\omega = 1$  keV. The compression pulse was followed by a shorter, higher frequency ignition pulse. The higher frequency pulse has negligible reflectivity and decreasing absorptivity, having  $\alpha_K = 10^6 \text{ cm}^{-1}$  at  $\hbar\omega = 20$  eV and  $\alpha_K = 10 \text{ cm}^{-1}$  at  $\hbar\omega = 1$  keV. If we take a higher frequency, shorter wavelength of 20 nm in the X-ray range then the absorptivity of the DT fuel is about  $\alpha_K = 10^4 \text{ cm}^{-1}$  (Hu *et al.*, 2014). This means that the full pulse energy is absorbed in  $10^{-4} \text{ cm} = 1 \mu\text{m}$ . That is in a thin surface layer. The internal domain is heated up due to adiabatic compression, up to ignition, but the major part of the approximately  $10 \mu\text{m}$  thin compressed surface layer remains cold and only  $1 \mu\text{m}$  is heated up at the outside surface. See Figure 8 of (Hu *et al.*, 2014).

**Compression shocks:** The final stage of compression both in direct (Boehly *et al.*, 2011) and indirect drive (Glenzer *et al.*, 2011) experiments was done by initiating 3–4 implosion shocks, well timed, so that all shocks converged to a final one with maximal speed. The fine timing of these shocks was based on the LASNEX and HYDRA non-RFD codes, which could describe “space-like” implosion shocks (i.e. shocks with space-like normal in the space–time). The final shock velocities reached  $1 - 1.25 \times 10^{-3} c$  in the National Ignition Champagne (Jones *et al.*, 2012; Landen *et al.*, 2012; Robey *et al.*, 2012), while recently with the initial “high foot” irradiation (Clark *et al.*, 2016) velocities reached  $1.6 \times 10^{-3} c$ .

**RFD:** These velocities are significantly less than the speed of light,  $c$ , so why would we need RFD to describe these reactions? RFD must be used not only with high velocities or high-velocity gradients but also at (A) radiation dominated processes, that is at very high temperatures, where the energy density and the pressure are of the same order of magnitude and not dominated by the rest mass of the matter. RFD has qualitatively different features, proven theoretically and experimentally: Detonation or burning fronts can be both space- and time-like (i.e. simultaneous in space–time) (Csernai, 1987) and in (B) radiation dominated processes, fluctuations of the burning front are smoothed out because radiation will transfer energy to volume elements with smaller energy density, which were created by mechanical flow fluctuations (Zeldovich and Raiser, 1966).

### Considerations for the target

In the following analytic, scaling consideration we could take (a) a compressed initial state of radius  $R$ , which is then not compressed further much, but heated up with a short penetrating light pulse. Alternatively, we could (b) consider a solid sphere of the same amount of DT fuel, which is then made transparent and ignited by a laser pulse without significant compression. In this second case due to the smaller density, we will need a more energetic short pulse but also longer time because of the larger size.

Jarrott *et al.* (2016) used a similar size target in a direct drive configuration, with an outer ablator layer and initial compression. These experiments did not achieve ignition; however, they used a special cone-in-shell configuration of the target. Through doping the target with Cu, they were able to project the  $K$ -shell radiation

of the target when it was radiated by an ultraviolet driver beam. From their images in Figure 2d, f of (Jarrott *et al.*, 2016), we see that ignition is achieved in an area of approximately  $50 \mu\text{m}$  radius from the center of the target. By using a high-contrast laser and a  $40 \mu\text{m}$  cone tip they were able to increase the fast electron coupling to the core from  $<5\%$  to  $10\text{--}15\%$  by an increase in the core-density and decrease in the source-to-core distance. If this laser-to-electron conversion efficiency would be further increased, the total laser energy coupled to the core would also increase above  $15\%$ , which may be good if we want to achieve fast-ignition inertial-confinement fusion.

Here we consider another configuration, without ablator layer and without too much pre-compression, using the early examples in (Csernai, 1987; Csernai and Strotzman, 2015). These estimates are based on an analytic, scaling solution of relativistic radiation dominated fluid dynamics, which demonstrates the consequences of this approach. The model parameters are given in terms of the pre-compressed pellet radius  $R$ , and the light penetration time across this pellet. These can be rescaled to any actual pre-compressed pellet size and fuel density at this time. To keep the transparency of the simple analytic scaling solution we describe a solid target, without a hole in it. To have some approximate quantitative result, we chose a target about  $640 \mu\text{m}$  radius, with a DT ice as fuel. The target density is taken to  $1.062 \text{ g/cm}^3$ , assuming that this is a pre-compressed density, which can be achieved still without the occurrence of RT instability. This target a priori has smaller absorptivity. If we want to absorb the whole energy of the incoming laser light on  $\sim 1.3 \text{ mm}$  length, we need an absorptivity of  $\alpha_K \approx 8 \text{ cm}^{-1}$ . This is about the absorptivity of DT fuel for soft X-ray radiation of  $1 \text{ nm}$  wavelength. See Figure 2 of (Hu *et al.*, 2014). Longer wavelength radiation would have a larger absorptivity, and would be absorbed in the outside layers of the pellet.

### Simplified model

Consider a spherical piece of matter ( $E$ ), which is sufficiently transparent for radiation. The absorptivity of the target matter is considered to be constant, such that the total energy of the incoming light is observed fully when the light reaches the opposite edge of the spherical target. This matter undergoes an exothermic reaction if its temperature exceeds  $T_c$ .

The target matter is surrounded by a set of spherically distributed laser beams, which emit the radiation necessary to heat up  $E$ . Here, for simplicity, we are neglecting the expansion of the outer shell inwards as well as the expansion of the core so that the core radius  $R$  is taken to be constant. We will measure the length in units of  $\mu\text{m}$ , and the time in units of  $\mu\text{m}/c$ .

We intend to calculate the temperature distribution,  $T(t, r)$ , within the sphere, as a function of time,  $t$ , and the radial distance from the center of the sphere, that is radius  $r$ . We have two steps of the evaluation:

- (i) In the first step, we calculate how much energy can reach a given point at  $r$  from the outside surface of the sphere. Here we have to take into account that the outside thermal radiation starts at time  $t = 0$ , so there is no radiation before. The eventual, “Low foot” type pre-compression is not included in this dynamical calculation. Furthermore, we must consider, which parts of the outside surface can reach a point inside the sphere at time  $t$ , and which are on the backward light-cone of the point at  $r$  and time  $t$ . The integral for

the energy density reaching the point from this part of the two-dimensional outside surface of the sphere in unit time interval,  $dt$ , is  $dU(t, r)/dt$ .

- (ii) Then we have to add up the accumulated radiation at position  $r$ , for the previously obtained energy and to obtain the time dependence of the temperature distribution,  $T(t, r)$ , we have to integrate  $dU(t, r)/dt$  from  $t = 0$ , for each spatial position.

We perform the surface integral of step (i) in terms of integration for the proper time of the radiation with a delta function, selecting the surface element, which can reach the given internal point at a time.

Let us study a point within the sphere, at a distance  $r$  from the center. Choose the  $x$ -axis passing through this point and the center of the sphere. See Figure 1.

The surface area of a ring of the sphere at the selected polar angle  $\Theta$  is  $dS = 2\pi R^2 \sin\Theta d\theta$ .

Step (i): At a point at  $r$  we receive radiation from a layer edge ribbon at time  $\tau$ . The radiation at distance  $\zeta$  is decreasing as  $1/\zeta^2$ . The total radiation reaching point  $r$  from the ribbon at  $\Theta$  is

$$dU(t, r) \propto \frac{1}{\zeta^2} \delta(\zeta - \sqrt{R^2 + r^2 - 2rR \cos \Theta}), \tag{1}$$

where  $\tau = \zeta/c$ , and we should integrate this for the surface of all ribbons.

The average intensity of thermal radiation reaching the surface of the pellet amounts to  $Q$  per unit surface ( $\mu\text{m}^2$ ) and unit time ( $\mu\text{m}/c$ ). Let us take a typical value for the energy of the total ignition pulse to be 2 MJ, in time 10 ps, then  $Q = 2\text{MJ} (4\pi)^{-1} (0.640 \mu\text{m})^{-2} (10 \text{ps})^{-1}$  or  $Q \approx 3.87 \times 10^{20}$ ,  $\text{W}/\text{cm}^2 = 1.29 \times 10^{10} \text{J}/\text{cm}^3$ .

Up to a given time  $t$ , the light can reach a space-time point  $(t, r)$ , inside the sphere from different points of the outside surface, which were emitted in different times. At early times it may be that none of the surface points are within the backward

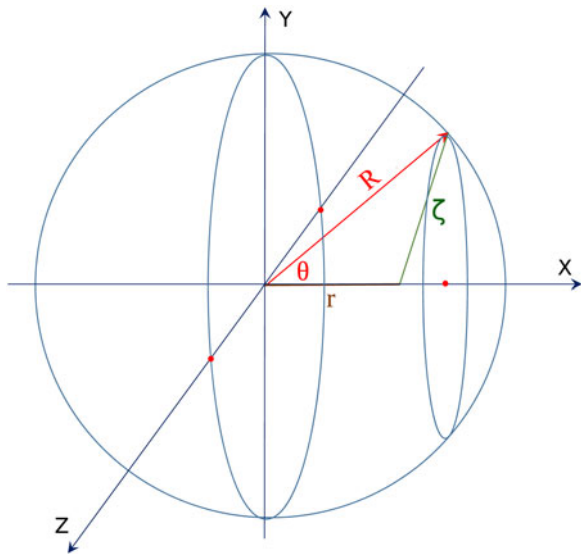


**Fig. 1.** The sphere of the fuel, with an internal point at the radius  $r$ . Let us chose the  $x$ -axis so that it passes through the point at  $r$  and the center of the sphere. Then let us chose a point on the sphere, and the angle of this point from the  $x$ -axis is denoted by  $\Theta$ . Then the length between this surface point and the internal point at  $r$  is  $\zeta = (R^2 + r^2 - 2Rr \cos\Theta)^{1/2}$ . The propagation time from the surface point to the point at  $r$  equals  $\tau = \zeta/c$ .

light-cone of the point  $(t, r)$ . At later times, from part of the surface points the light can reach  $(t, r)$ , while at times larger than  $2R/c$  all internal points can be reached from any surface point of the sphere. Thus, we calculate first what energy density,  $U(t, r)$ , we get at a space-time point  $(t, r)$ , from earlier times. At a given point at  $R$  measured from the center of the sphere (assuming that a constant fraction,  $\alpha_K$ , of the radiation energy is absorbed in unit length):<sup>1</sup>

$$\begin{aligned} dU(t, r) &= \alpha_K Q \int_0^t d\tau 2\pi R^3 \\ &\times \int_0^\pi d\cos\Theta \frac{\delta(\zeta - \sqrt{R^2 + r^2 - 2rR \cos\Theta})}{R^2 + r^2 - 2rR \cos\Theta} \\ &= \alpha_K Q \int_0^t d\tau 2\pi R^3 \int_1^{-1} dx \frac{\delta(\zeta - \sqrt{R^2 + r^2 - 2rRx})}{R^2 + r^2 - 2rRx} \\ &= 2\pi R^3 \alpha_K Q \cdot (Rr)^{-1} \int_{(R-r)/c}^{aR/c} \frac{d\tau}{\tau c}, \end{aligned} \tag{2}$$

where the integral over  $dx$  gives  $1/(Rr\zeta) = (Rr\tau c)^{-1}$ . The time,  $d\tau$ , integral runs from the nearest point of the backward light cone to the surface of the sphere to the furthest point,  $aR/c$ . Here the parameter  $a$  will be described later. See Figure 2.

Now we introduce a new, dimensionless time variable:  $q \equiv \tau c/R$ . Thus,

$$\begin{aligned} dU(t, r) &= 2\pi R^3 \alpha_K Q \cdot (rRc)^{-1} \\ \int_{1-r/R}^a \frac{dq}{q} &= 2\pi R^2 \alpha_K Q \cdot (rc)^{-1} [\ln(q)]_{1-r/R}^a, \end{aligned} \tag{3}$$

where  $\zeta = \tau c$  and  $a$  is the upper boundary of the integral over the dimensionless time  $dq$ .

$$a = \begin{cases} 1 - r/R, & q < 1 - r/R \\ q, & 1 - r/R < q < 1 + r/R \\ 1 + r/R, & q > 1 + r/R. \end{cases} \tag{4}$$

Here actually the integral over  $dq$  is adding up the contributions of those surface elements of the sphere, from where radiation reaches the internal point at  $r$  at the same dimensionless time  $q$ . In the first case, the radiation does not reach the point at  $r$  then, in the second part, the radiation from the closest point of the sphere reaches  $r$  but from the opposite point not yet, in the third case radiation reaches  $r$  from all sides.

Thus the energy deposited in unit time at a dimensionless time  $q$  is

$$\begin{aligned} dU(r, q) &= \frac{2\pi R^2 \alpha_K Q}{rc} \times \\ &\begin{cases} \ln[(1 + r/R)/(1 - r/R)], & q > 1 + r/R \\ \ln[q/(1 - r/R)], & 1 - r/R < q < 1 + r/R \\ 0, & q < 1 - r/R. \end{cases} \end{aligned} \tag{5}$$

<sup>1</sup>We are using the relation  $\delta[g(x)] = \sum_i [1/|g'(a_i)|] \delta(x - a_i)$  where  $a_i$ -s are the roots of  $g(x) = \zeta - \sqrt{R^2 + r^2 - 2rRx}$ , that is  $g(a_i) = 0$ . Now  $a_1 = (R^2 + r^2 - \zeta^2)/(2rR)$  and  $g'(x) = rR/\zeta$  so that the integrand is  $\zeta/(\zeta^2 rR) = 1/(rR\zeta)$ . The variable  $\zeta$  depends on  $x$  (or  $\Theta$ ), so we should set the integral boundaries in terms of  $\zeta$  accordingly.

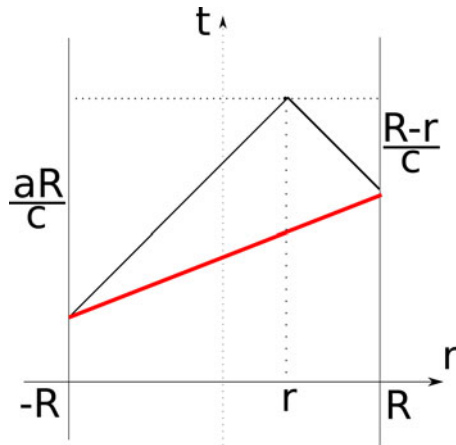


**Fig. 2.** The boundaries of the integration domains depending on  $r$  and  $t$ . The domain for the smallest  $\tau$ -values cannot receive radiation, Eq. (2), because the radiation started at  $(R - r)/c$  earlier and it reaches the internal point at  $r$  later. At the same time, the radiation from the opposite side reaches the point  $r$  also in time  $aR/c$ . The contour of the intersection of the backward light-cone with the surface of the sphere is indicated with the thick, red line. When the time from the momentum of ignition is longer than  $t = 2R/c$  the radiation reaches the matter from all sides at every location  $r$ . At earlier times the upper boundary of integration should be evaluated. See Equation (4).

Step (ii): Neglecting the compression and assuming constant specific heat  $c_v$ , we get that  $k_B dT = 1/nc_v dU \cdot dq$ , where  $k_B$  is the Boltzmann constant, and so

$$k_B T(t, r) = \frac{1}{nc_v} \int_0^{tc/R} dq \cdot dU(r, q) = \frac{2\pi R^2 \alpha_K Q}{nc_v rc} \times \begin{cases} [q \ln(1+r/R)/(1-r/R)]_{1+r/R}^{tc/R} \\ + (1+r/R) \ln[(1+r/R)/(1-r/R)] - 2r/R, & \text{if: } tc/R > 1+r/R \\ [q \ln(q/(1-r/R)) - q]_{1-r/R}^{tc/R}, & \text{if: } 1-r/R < tc/R < 1+r/R \\ 0, & \text{if: } tc/R < 1-r/R \end{cases} \quad (6)$$

and so,

$$k_B T(t, r) = H \cdot \frac{R^2}{r} \times \begin{cases} tc/R \ln[(1+r/R)/(1-r/R)] - 2r/R, & \text{if: } tc/R > 1+r/R \\ tc/R \ln[tc/(R/(1-r/R))] - tc/R + 1-r/R, & \text{if: } 1-r/R < tc/R < 1+r/R \\ 0, & \text{if: } tc/R < 1-r/R, \end{cases} \quad (7)$$

where the number density of uncompressed DT ice is  $n = 3.045 \times 10^{22} \text{ cm}^{-3}$ , and the leading constant,  $H$ , is

$$H \equiv \frac{2\pi Q}{cc_v} \frac{\alpha_K(r)}{n} = 8.54 \times 10^{-12} \text{ J/cm}. \quad (8)$$

If the absorptivity is varying,  $\alpha_K = \alpha_K(r)$ , then it follows:

$$k_B T(t, r) = \frac{2\pi QR}{cc_v n} \begin{cases} 0, & \text{if: } tc < R - r \\ \frac{\alpha_K(r)tc}{r} \left( \ln \frac{tc}{R-r} - 1 \right) + \frac{R-r}{r}, & \text{if: } R-r < tc < R+r \\ \frac{\alpha_K(r)tc}{r} \ln \frac{R+r}{R-r} - 2, & \text{if: } tc > R+r. \end{cases} \quad (9)$$

The surface of the discontinuity is characterized by the  $T(t, r) = T_c$  contour line. If  $T_c$  is the ignition temperature, then here the DT ignition takes place on this contour line in the space-time. The tangent of this line is if  $tc > R + r$ :

$$\left( \frac{\partial r}{\partial t} \right)_{T_c} = \left( \frac{\partial T}{\partial t} \right)_{T_c} / \left( \frac{\partial T}{\partial r} \right)_{T_c} = \frac{R+r/R-r}{\ln \left\{ \frac{tc(2R/R^2 - r^2) + [(\alpha'_K(r)/\alpha_K(r)) - (1/r)]}{\ln(R+r/R-r)} \right\}} \quad (10)$$

So the point  $(t_c, r_c)$  where the space- and time-like parts of the surface meet, from  $(\partial r / (\partial t))_{T_c} = 1$  is

$$t_c = \left\{ \frac{2cR}{R^2 - r_c^2} \left[ \ln \frac{R+r_c}{R-r_c} \right]^{-1} + \left( \frac{\alpha'_K(r)}{\alpha_K(r)} - \frac{c}{r_c} \right) \right\}^{-1}. \quad (11)$$

This line  $t = t_c(r_c)$  separates the space- and time-like branch of the discontinuity of  $T(t, r) = T_c$ .

The discontinuity initiates at  $r = R$  and  $t = 0$  and it propagates first slowly inwards. Due to the radiative heat transfer the contour line of ignition,  $T(t, r) = T_c$ , accelerates inwards, and at  $r_c = r_c(T_c)$  it develops smoothly from space-like into a time-like discontinuity.

The same type of gradual development from space-like into time-like detonation (A) occurs in the last, *hadronization*, phase of ultra-relativistic heavy ion collisions (Csernai, 1994; Heinz and Kolb, 2002; Chatterjee et al., 2006; Frodermann et al., 2007; Molnar et al., 2007; Csernai et al., 2009; Armesto et al., 2014; Floerchinger and Wiedemann, 2014). If we include radiative heat transfer in these scenarios, the transition from space- to time-like deflagration will be gradual. This, however, requires more involved numerical calculations.

In Figure 3, we see the constant temperature contour lines,  $T(t, r) = \text{const.}$ , in the space-time, from the analytical solution. For the first or second  $T = \text{const.}$  contour line the time-like detonation region extends from the center of the pellet to the half of radius  $R$ . This is only about 12% of the volume, so the time-like detonation, in itself, cannot achieve total simultaneous volume ignition, and in the outside region instabilities might develop!

### Variable absorptivity

In order to study the effect of variable absorptivity, we reformulated the numerical model to perform all integrals of the model numerically. This will enable us to study the configuration where the pellet is manufactured with nano-shells inside, which regulate the absorptivity of the DT ice pellet.

At first, we still assumed constant absorptivity with the same value  $\alpha_K = 8 \text{ cm}^{-1}$ . In Figure 4, the numerical solution gives a

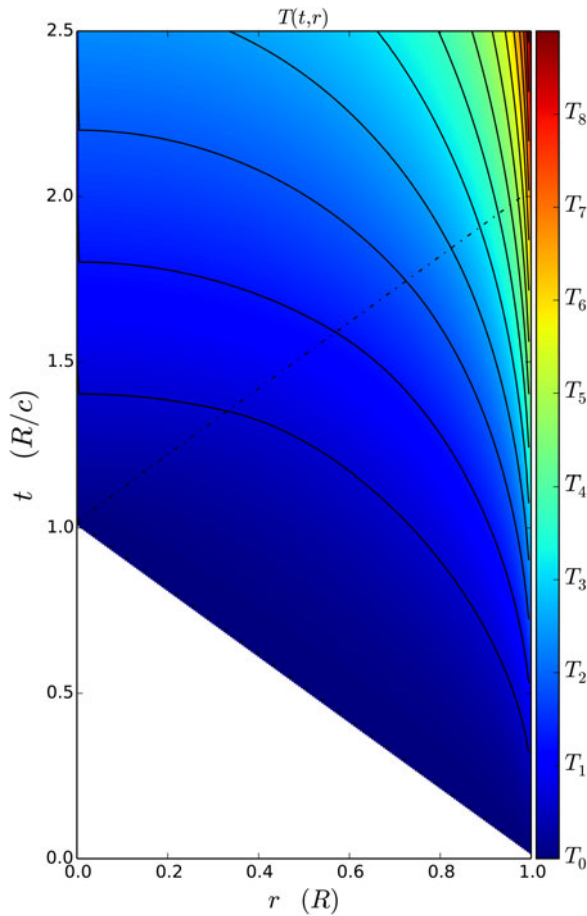


**Fig. 3.** Analytic solution of the radiation dominated implosion model of rapid ignition. The temperature distribution in function of distance and time. The lower boundary and the dotted line represent the light cones from the left and right edge of the pellet, initiated at  $t=0$ . The absorptivity of the pellet is  $\alpha_K = 8 \text{ cm}^{-1}$ . The temperature is measured in units of  $T_1 = H \cdot R = 21.3 \text{ keV}$ , and  $T_n = n \cdot T_1$ .

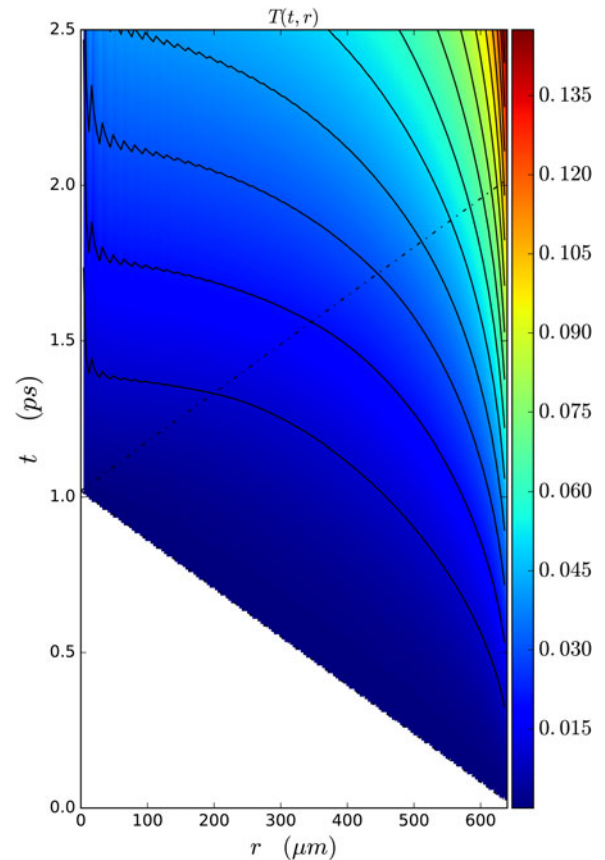


**Fig. 4.** Numerical solution of the radiation dominated implosion model of rapid ignition. The temperature distribution in function of distance and time. The dotted line represents the light cone. The absorption coefficient is constant  $\alpha_K = 8 \text{ cm}^{-1}$ . The decrease of radiation flux due to the absorption is neglected. The temperature is measured in units of  $T_1 = H \cdot R = 21.3 \text{ keV}$ , and  $T_n = n \cdot T_1$ . The finite numerical resolution leads to the fluctuations near  $r=0$ . The color code for the temperature,  $T(t, r)$ , is given in units of (MeV).

qualitatively identical result, but at small radii, the numerical uncertainty leads to visible fluctuations and somewhat smaller central temperature increase. The domain of time-like, that is simultaneous ignition takes place in the central part of the pellet up to a radius of  $r = 370 \text{ }\mu\text{m}$ .

In Hu *et al.* (2014), Rochester and NIF experimental data were studied and analyzed with opacity data, extracted both from basic principles and from comparison with ICF experiments. The absorption coefficient  $\alpha_K \text{ (cm}^{-1}\text{)}$ , defined by  $I(x) = \exp(-\alpha_K x)I_0$ , and the Rosseland and Planck opacities,  $K_R$  defined by  $I(x) = \exp(-\alpha_{K_R} \rho x)I_0$ , were estimated and used to simulate the space–time development of ICF direct ignition experiments.

In our previous calculations, we used the absorption coefficient  $\alpha_K \text{ (cm}^{-1}\text{)}$ , and the approximation that the intensity of the incoming laser light flux is sufficiently large so that its decrease by the absorption is negligible.

With increased absorptivity, one could reach more rapid heating. The fusion reaction rate per unit volume and unit time is  $f = n_D n_T \langle \sigma v \rangle$ , depends on the D and T densities,  $n_D n_T$ , and the reactivity,  $\langle \sigma v \rangle$ . Due to the fusion cross-section, the reactivity is increasing up to about  $T = 70\text{--}100 \text{ keV}$ , and then decreases again. Thus, we could aim for a heating up to this temperature, with smaller pre-compression.

### Variation of absorptivity by Nanotechnology

Doping INF pellets with golden nano-shells enables us to achieve the desired variable absorptivity (Tanabe, 2016). Nano-shells irradiated by laser light exhibit a resonant light absorption, which can increase the plasmon field-strength by up to a factor of 40–100 or more (Prodan *et al.*, 2003; Nordlander and Prodan 2004). At present experimentally realizable nano-shell sizes ranges for core sizes: 5–500 nm, and for shell thickness: 1–100 nm. In a fuel target prepared initially with implanted Au nano-shells, after pre-compression, we can have nano-shells of a radius  $\approx 10 \text{ nm}$ .

The resonant light frequency of the nano-shell can be tuned in a very wide range by changing the size and thickness of the nano-shell. If the core ( $r_1$ ) versus the shell thickness,  $r_1/(r_2 - r_1)$  is changed from 2 to 800 the resonant wavelength changed from 0.5 to  $10 \times 10^3 \text{ nm}$  (Loo *et al.*, 2004). For our purposes of short wavelength, X-ray photons the smaller and relatively more thick nano-shells are relevant. An eventual pre-compression modifies the nano-shells in this direction.

At the resonant frequencies, the nano-shells are able to absorb resonantly a rather high portion of incoming light. We can define the absorption, scattering, and extinction efficiencies,  $Q_{\text{abs}}$ ,  $Q_{\text{scat}}$ , and  $Q_{\text{ext}}$ , respectively (Lee and El-Sayed, 2005), where these coefficients,  $Q_i$ , describe how much part of the energy of the incoming light is

absorbed or scattered by the nano-shell, compared with its geometrical cross-section,  $G$ , that is for a sphere of radius  $R$ ,  $G = R^2 \pi$ .

The nano-shells can be tuned to either larger absorption efficiency or larger scattering efficiency. For our purposes, the larger absorption efficiency is optimal. The resonance extinction or absorption efficiency can reach a factor 10 or even more (Alam and Massoud, 2006).

Thus, the absorptivity of the target material of the pellet can be regulated by the density of implanted nano-shells. The target DT fuel has a bulk absorption coefficient,  $\alpha_{k0}$  ( $\text{cm}^{-1}$ ). If we implant nano-shells with cross-section  $G = R^2 \pi$ , with a density  $\rho$  ( $\text{cm}^{-3}$ ) then the absorptivity will increase to

$$\alpha_k = \alpha_{k0} + \alpha_{\text{ns}}, \tag{12}$$

where the absorptivity of nano-shells,  $\alpha_{\text{ns}}$ , is

$$\alpha_{\text{ns}} = \rho G Q_{\text{abs}}. \tag{13}$$

For a nano-shell of  $R = 30$  nm the additional contribution would be  $\rho G Q_{\text{abs}} = \rho Q_{\text{abs}} 0.283 \text{ cm}^2$ . Consequently, for a typical nano-shell density (James *et al.*, 2007) of  $\rho = 10^{11}/\text{cm}^3$  and a  $Q_{\text{abs}} \approx 10$ , we can reach an additional absorptivity of

$$\alpha_{\text{ns}} = 28.3 \text{ cm}^{-1}. \tag{14}$$

Higher nano-shell density and higher absorption efficiency can also be achieved. A pre-compression of the target fuel would further increase the absorptivity.

Absorption for DT densities in the range of  $\rho = 5 - 200 \text{ g/cm}^3$ ,  $T \approx 10^5 \text{ K}$  were obtained in the range of

$$\alpha_{k0} = 10^{-1} - 10 \text{ cm}^{-1}$$

as the light frequency increased to  $\hbar\omega = 1 - 10 \text{ keV}$ . That is the typical light mean free path was about  $1 - 10^4 \mu\text{m}$ . Thus, while for low-frequency radiation,  $\hbar\omega = 1 - 100 \text{ eV}$  the DT target is quite opaque, at higher frequencies or energy it is much more transparent. This leads to the result that the initial lower energy pulse leads primarily to compression. This effect is enhanced further with the application of the thin ablator sheet on the surface of the pellet (Benredjem *et al.*, 2014).

The additional opacity of nano-shells with typical nano-shell densities can increase the absorptivity by up to

$$\alpha_{\text{ns}} = 20 - 30 \text{ cm}^{-1},$$

which makes the fast ignition possibilities very versatile in this light frequency range. We can experiment with variable absorptivity, which is the normal high-temperature, high-frequency absorptivity of the DT fuel,  $\alpha_{k0} \approx 1 \text{ cm}^{-1}$  at the outer edge of the pellet (i.e. at  $R = 640 \mu\text{m}$ ) while in the center, it is  $\alpha_{\text{ns}} = 20 - 30 \text{ cm}^{-1}$  (i.e. about up to 30 times more). The space-time profile of the ignition will then depend on the radial profile of the increasing nano-shell doping toward the center of the pellet.

We could optimize this by achieving the largest simultaneous volume ignition domain, which eliminates the possibility of developing instabilities.

Here the question arises that under compression of a sample doped with nano-shells, how the doped particles will compress. The thickness and radius of the golden nano-shells are

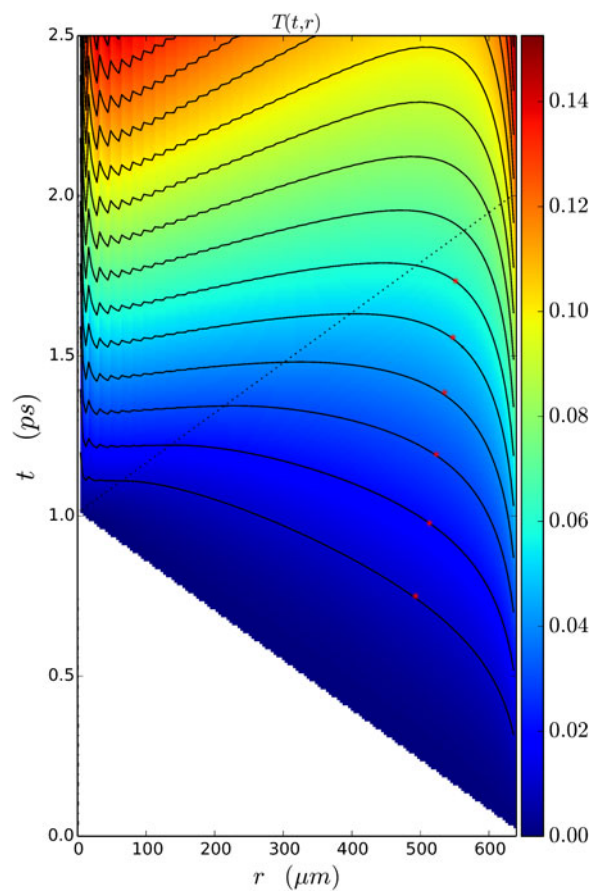


**Fig. 5.** Numerical solution of the radiation dominated implosion model of rapid ignition. The temperature distribution in function of distance and time. The dotted lines represent the light cone. The absorption coefficient is linearly changing with the radius. In the center,  $r=0$ ,  $\alpha_k = 30 \text{ cm}^{-1}$  while at the outside edge  $\alpha_k = 8 \text{ cm}^{-1}$ . The decrease of radiation flux due to the absorption is neglected. The temperature is measured in units of  $T_1 = H \cdot R = 21.3 \text{ keV}$ , and the  $T_n(r) = n \cdot T_1 = \text{const.}$  contour lines are shown. The color code for the temperature,  $T(t, r)$ , is given in units of (MeV). The finite numerical resolution leads to the fluctuations near  $r=0$ , this is a numerical artifact. The stars on the temperature contour lines indicate the transition from the space-like front at the outside edge to the time-like front in the middle. The points of the middle part are not causally connected, so instabilities cannot develop.

determined by the resonance condition of the laser irradiation. The stiffness of the shell interior can be chosen to keep the spherical shape of the nano-particles, the best choice can be cryogenic DT fluid. In a study of ICF capsules employing DT-wetted foam (Sacks and Darling, 1987) of similar size small pores, concluded that the inflight aspect ratio, hydrodynamic efficiency, and hot electron tolerance can be at least as good as for conventional DT targets. The compressed nano-shells will be resonant to higher laser frequencies, which can be taken into account, in the nano-shell fabrication.

### Conclusions and discussions

Using nano-technology for ICF is mentioned recently (Kaymak *et al.*, 2016; Bargstenm *et al.*, 2017). By placing aligned nano-rods or nano-wires on the surface of the pellet and irradiating it with femtosecond laser pulses of relativistic intensity, leads to a plasma with peak electron intensity and pressure. However, this pressure would lead to a pressure-driven adiabatic compression and heating, which can lead to RT instabilities, preventing simultaneous volume ignition.

In this model estimate, we have neglected the compression of the target solid fuel ball, as well as the reflectivity of the target matter. The relatively small absorptivity made it possible that the radiation could penetrate the whole target. With the model parameters, we used the characteristic temperature was  $T_1 = 21.3$  keV, which is larger than the usually assumed ignition temperature, while our target is not compressed so the higher temperatures may be necessary to reach ignition according to the Lawson criterion. If we can achieve ignition at somewhat lower temperature than  $T_1$ , the ignition surface in the space-time includes a substantial time-like hyper-surface, where instabilities cannot develop because neighboring points are not causally connected.

From looking at the constant temperature contour lines in function of distance and time (Fig. 5), we see that the detonation at a higher critical temperatures  $T_c \approx T_4 - T_6$  occurs when the radiation reaches the matter from the other side also at  $t_c \approx 1.5$  ps. At these contour lines of  $T \approx 70 - 90$  keV, about the interior 90% of the radius ignites at the same time (A), so the ignition is simultaneous for about 73% of the total volume. In this domain, no instabilities may occur.

We can also apply this model is to a pre-compressed, more dense target, which is transparent and has larger absorptivity. In this situation, the ignition temperature can be somewhat smaller, but we still can optimize the pulse strength and pulse length to achieve the fastest complete ignition of the target.

The above relatively short and very intensive irradiation is relevant for the absolute boundary of simultaneous, time-like ignition (A). With more detailed and quantitative estimate it is sufficient to require an irradiation intensity, which leads to a faster temperature increase towards  $T_c$  than the growth rate of the RT instability or other instabilities. This can make even an order of magnitude increase in the critical irradiation time  $T_c$ . Furthermore, if we also consider the smoothing effect of radiation dominated ignition front (B) then the critical irradiation time even longer. This could only be estimated with a 3 + 1D Computational RFD calculation.

We can see if we neglect the importance of the speed of light, the theory would be far-fetched from reality. It is important to use the proper relativistic treatment to optimize the fastest, more complete ignition, with the least possibility of instabilities, which reduce the efficiency of ignition.

**Acknowledgements.** Enlightening discussions with Igor Mishustin and Horst Stöcker are gratefully acknowledged. This work is supported in part by the Institute of Advance Studies, Köszeg, Hungary.

## References

- Alam M and Massoud Y (2006) A closed-form analytical model for single nanoshells. *IEEE Transactions on Nanotechnology* 5, 265.
- Armesto N, Dainese A, d'Enterrria D, Masciocchi S, Roland C, Salgado CA, van Leeuwen A and Wiedemann UA (2014) Heavy-ion physics studies for the future circular collider. *Nuclear Physics A* 931, 1163.
- Bargsten C, Hollinger R, Capeluto MG, Kaymak V, Pukhov A, Wang SJ, Rockwood A, YWang Y, Keiss D, Tommasini R, London R, Park J, Busquet M, Klapisch M, Shlyaptsev VN and Rocca JJ (2017) Energy penetration into arrays of aligned nanowires irradiated with relativistic intensities: scaling to Terabar pressures. *Science Advances* 3, e1601558.
- Benredjem D, Pain JC, Gilleron F, Ferri S and Calisti A (2014) Opacity profiles in inertial confinement fusion. *Journal of Physics: Conference Series* 548, 012009.
- Betti R and Hurricane OA (2016) Inertial-confinement fusion with lasers. *Nature Physics* 12, 435.
- Boehly TR, Goncharov VN, Seka W, Barrios MA, Celliers PM, Hicks DG, Collins GW, Hu SX, Marozas JA, and Meyerhofer DD (2011) Velocity and timing of multiple spherically converging shock waves in liquid deuterium. *Physical Review Letters* 106, 195005.
- Chatterjee R, Frodermann ES, Heinz U and Srivastava DK (2006) Elliptic flow of thermal photons in relativistic nuclear collisions. *Physical Review Letters* 96, 202302.
- Clark DS, Marinak MM, Weber CR, Eder DC, Haan SW, Hammel BA, Hinkel DE, Jones OS, Milovich JL, Patel PK, Robey HF, Salmonson JD, Sepke SM and Thomas CA (2015) Radiation hydrodynamics modeling of the highest compression inertial confinement fusion ignition experiment from the National Ignition Campaign. *Physics of Plasmas* 22, 022703.
- Clark DS, Weber CR, Milovich JL, Salmonson JD, Kritcher AL, Haan SW, Hammel BA, Hinkel DE, Hurricane OA, Jones OS, Marinak MM, Patel PK, Robey HF, Sepke SM and Edwards MJ (2016) Three-dimensional simulations of low foot and high foot implosion experiments on the National Ignition Facility. *Physics of Plasmas* 23, 056302.
- Csernai LP (1987) Detonation on a time-like front for relativistic systems. *Zhurnal Eksperimental'noi i Teoreticheskoi Fiziki* 92, 379–386.
- Csernai LP (1994) *Introduction to Relativistic Heavy Ion Collisions*. Cichester, England: John Wiley & Sons.
- Csernai LP and Strottman DD (2015) Volume ignition via time-like detonation in pellet fusion. *Laser and Particle Beams* 33, 279–282.
- Csernai LP, Kroo N and Papp I (2017) Procedure to improve the stability and efficiency of laser-fusion by nano-plasmonics method. Patent # P1700278/3 of the Hungarian Intellectual Property Office.
- Csernai LP, Cheng Y, Horvat S, Magas V, Strottman D and Zétényi M (2009) Flow analysis with 3-dim ultra-relativistic hydro. *Journal of Physics G* 36, 064032.
- Floerchinger S and Wiedemann UA (2014) Kinetic freeze-out, particle spectra, and harmonic-flow coefficients from mode-by-mode hydrodynamics. *Physical Review C* 89, 034914.
- Frodermann E, Chatterjee R and Heinz U (2007) Evolution of pion HBT radii from RHIC to LHC – Predictions from ideal hydrodynamics. *Journal of Physics G* 34, 2249.
- Glenzer SH *et al.* (2011) Demonstration of ignition radiation temperatures in indirect-drive inertial confinement fusion hohlraums. *Physical Review Letters* 106, 085004.
- Haan SW, Lindl JD, Callahan DA, Clark DS, Salmonson JD, Hammel BA, Atherton LJ, Cook RC, Edwards MJ, Glenzer S, Hamza AV, Hatchett SP, Herrmann MC, Hinkel DE, Ho DD, Huang H, Jones OS, Kline J, Kyrala G, Landen OL, MacGowan BJ, Marinak MM, Meyerhofer DD, Milovich JL, Moreno KA, Moses EI, Munro DH, Nikroo A, Olson RE, Peterson K, Pollaine SM, Ralph JE, Robey HF, Spears BK, Springer PT, Suter LJ, Thomas CA, Town RP, Vesey R, Weber SV, Wilkens HL and Wilson DC (2011) Point design targets, specifications, and requirements for the 2010 ignition campaign on the National Ignition Facility. *Physics of Plasmas* 18, 051001.
- Heinz UW and Kolb PF (2002) Emission angle dependent pion interferometry at RHIC and beyond. *Physics Letters B* 542, 216.
- Hu SX, Collins LA, Goncharov VN, Boehly TR, Epstein R, McCrory RL and Skupsky S (2014) First principle opacity table of warm dense deuterium for inertial-confinement-fusion applications. *Peer-Reviewed Journal* 90, 033111.
- James WD, Hirsch LR, West JL, O'Neal PD and Payne JD (2007) Application of INAA to the build-up and clearance of gold nanoshells in clinical studies in mice. *The Journal of Radioanalytical and Nuclear Chemistry* 271, 455–459.
- Jarrott LC, Wei MS, McGuffey C, Solodov AA, Theobald W, Qiao B, Stoeckl C, Betti R, Chen H, Delettrez J, Döppner T, Giraldez EM, Glebov VY, Habara H, Iwawaki T, Key MH, Luo RW, Marshall FJ, McLean HS, Mileham C, Patel PK, Santos JJ, Sawada H, Stephens RB, Yabuuchi T and Beg FN (2016) Visualizing fast electron energy transport into laser-compressed high density fast-ignition targets. *Nature Physics* 12, 499.
- Jones OS, Cerjan CJ, Marinak MM, Milovich JL, Robey HF, Springer PT, Benedetti LR, Bleuel DL, Bond EJ, Bradley DK, Callahan DA, Caggiano JA, Celliers PM, Clark DS, Dixit SM, Doppner T, Dylla-Spears RJ, Dzentitis EG, Farley DR, Glenn SM, Glenzer SH, Haan SW, Haid BJ, Haynam CA, Hicks DG, Koziemiński BJ, LaFortune KN, Landen OL, Mapoles ER, MacKinnon AJ, McNaney JM,

- Meezan NB, Michel PA, Moody JD, Moran MJ, Munro DH, Patel MV, Parham TG, Sater JD, Sepke SM, Spears BK, Town RPJ, Weber SV, Widmann K, Widmayer CC, Williams EA, Atherton LJ, Edwards MJ, Lindl JD, MacGowan BJ, Suter LJ, Olson RE, Herrmann HW, Kline JL, Kyrala GA, Wilson DC, Frenje J, Boehly TR, Glebov V, Knauer JP, Nikroo A, Wilkens H and Kilkenny JD (2012) A high-resolution integrated model of the National Ignition Campaign cryogenic layered experiments. *Physics of Plasmas* **19**, 056315.
- Kaymak V, Pukhov A, Shlyaptsev VN and Rocca JJ (2016) Nano-scale ultra-dense Z-pinches formation from laser-irradiated nanowire arrays. *Physical Review Letters* **117**, 035004.
- Landen OL, Benedetti R, Bleuel D, Boehly TR, Bradley DK, Caggiano JA, Callahan DA, Celliers PM, Cerjan CJ, Clark D, Collins GW, Dewald EL, Dixit SN, Doepfner T, Edgell D, Eggert J, Farley D, Frenje JA, Glebov V, Glenn SM, Glenzer SH, Haan SW, Hamza A, Hammel BA, Haynam CA, Hammer JH, Heeter RE, Herrmann HW, Hicks DG, Hinkel DE, Izumi N, Gatu Johnson M, Jones OS, Kalantar DH, Kauffman RL, Kilkenny JD, Kline JL, Knauer JP, Koch JA, Kyrala GA, LaFortune K, Ma T, Mackinnon AJ, Macphree AJ, Mapoles E, Milovich JL, Moody JD, Meezan NB, Michel P, Moore AS, Munro DH, Nikroo A, Olson RE, Opachich K, Pak A, Parham T, Patel P, Park H-S, Petrasso RP, Ralph J, Regan SP, Remington BA, Rinderknecht HG, Robey HF, Rosen MD, Ross JS, Salmonson JD, Sangster TC, Schneider MB, Smalyuk V, Spears BK, Springer PT, Suter LJ, Thomas CA, Town RPJ, Weber SV, Wegner PJ, Wilson DC, Widmann K, Yeaman C, Zylstra A, Edwards MJ, Lindl JD, Atherton LJ, Hsing WW, MacGowan BJ, Van Woutherghem BM and Moses EI (2012) Progress in the indirect-drive National Ignition Campaign. *Plasma Physics and Controlled Fusion* **54**, 124026.
- Lee K-S and El-Sayed MA (2005) Dependence of the enhanced optical scattering efficiency relative to that of absorption for gold metal nanorods on aspect ratio, size, end-cap shape and medium refractive index. *Journal of Physical Chemistry B* **109**, 20331–20338.
- Lindl JD (1998) *Inertial Confinement Fusion*. New York: Springer.
- Lindl JD, Amendt P, Berger RL, Glendinning SG, Glenzer SH, Haan SW, Kauffman RL, Landen OL and Suter LJ (2004) The physics basis for ignition using indirect-drive targets on the National Ignition Facility. *Physics of Plasmas* **11**, 339.
- Loo C, Lin A, Hirsch L, Lee M.-H., Barton J, Halas N, West J and Drezek R (2004) *Nanoshell-Enabled Photonics-Based Imaging and Therapy of Cancer, Technology in Cancer Research & Treatment* (ISSN 1533-0346) 3 (1). Schenectady, NY, USA: Adenine Press.
- Molnar E, Molnar E, Csernai LP, Magas VK, Lazar ZI, Nyiri A and Tamosiunas K (2007) Covariant description of kinetic freeze-out through a finite time-like layer. *Journal of Physics G* **34**, 1901.
- Nora R, Theobald W, Betti R, Marshall FJ, Michel DT, Seka W, Yaakobi B, Lafon M, Stoeckl C, Delettrez J, Solodov AA, Casner A, Reverdin C, Ribeyre X, Vallet A, Peebles J, Beg FN and Wei MS (2015) Gigabar Spherical Shock Generation on the OMEGA Laser. *Physical Review Letters* **114**, 045001.
- Nordlander P and Prodan E (2004) Plasmon hybridization in nanoparticles near metallic surfaces. *Nano Letters* **4**, 2209–2231.
- Prodan E, Radloff C, Halas NJ and Nordlander P (2003) A hybridization model for the plasmon response of Complex Nanostructures. *Science* **301**, 419–422.
- Reis VH, Hanrahan RJ and Levedahl WK (2016) The big science of stockpile stewardship. *Physics Today* **69**, 46.
- Robey HF, Boehly TR, Celliers PM, Eggert JH, Hicks D, Smith RF, Collins R, Bowers MW, Krauter KG, Datte PS, Munro DH, Milovich JL, Jones OS, Michel PA, Thomas CA, Olson RE, Pollaine S, Town RPJ, Haan S, Callahan D, Clark D, Edwards J, Kline JL, Dixit S, Schneider MB, Dewald EL, Widmann K, Moody JD, Doppner T, Radousky HB, Throop A, Kalantar D, DiNicola P, Nikroo A, Kroll, JJ, Hamza AV, Horner JB, Bhandarkar SD, Dzenitis E, Alger E, Giraldez E, Castro C, Moreno K, Haynam C, LaFortune KN, Widmayer C, Shaw M, Jancaitis K, Parham T, Holunga DM, Walters CF, Haid B, Mapoles ER, Sater J, Gibson CR, Malsbury T, Fair J, Trummer D, Coffee KR, Burr B, Berzins LV, Choate C, Brereton SJ, Azevedo S, Chandrasekaran H, Eder DC, Masters ND, Fisher AC, Sterne PA, Young BK, Landen OL, Van Woutherghem BM, MacGowan BJ, Atherton J, Lindl JD, Meyerhofer DD and Moses E (2012). Shock timing experiments on the National Ignition Facility: initial results and comparison with simulation. *Physics of Plasmas* **19**, 042706.
- Sacks RA and Darling DH (1987) Direct drive cryogenic ICF capsules employing D-T wetted foam. *Nuclear Fusion* **27**, 447.
- Tanabe K (2016) Plasmonic energy nanofocusing for high-efficiency laser fusion ignition. *Japanese Journal of Applied Physics* **55**, 08RG01.
- Zeldovich YB and Raiser YP (1966) *Physics of Shock Waves and High-Temperature Hydrodynamic Phenomena*. Moscow: Nauka.